

Article

Suppression of Radiated Emissions from Inductive-Resonant Wireless Power Transfer Systems by Using Spread-Spectrum Technique

Deniss Stepins ^{1,*}, Janis Zakis ¹ , Padmapriya Padmanaban ² and Dhruv Deveshkumar Shah ²

¹ Institute of Industrial Electronics and Electrical Engineering, Riga Technical University, 1048 Riga, Latvia; janis.zakis@rtu.lv

² Institute of Radio Electronics, Riga Technical University, 1048 Riga, Latvia; padmapriya.padmanaban@edu.rtu.lv (P.P.); shahdhruv1411@gmail.com (D.D.S.)

* Correspondence: deniss.stepins@rtu.lv

Abstract: Inductive-resonant wireless power transfer systems are often used for wireless transfer of electric power. However, they are significant sources of radiated electromagnetic emissions. The effect of spread-spectrum approach based on classical switching frequency modulation of inductive-resonant wireless power transfer system inverter operating frequency and multi-frequency technique on the radiated emissions and efficiency is studied experimentally in detail. The influence of the classical frequency modulation and multi-frequency technique parameters on the peak radiated emission levels and the efficiency of the inductive-resonant wireless power transfer system are investigated more comprehensively. It is shown in the paper that the spread-spectrum approaches can lead to an appreciable radiated emissions reduction with small or large impact on the system's efficiency. Some useful recommendations on how to choose parameters of the periodic switching frequency modulation or the multi-frequency technique considering a trade-off between the radiated emissions reduction and the efficiency are also proposed.

Keywords: wireless power transfer; inductive-resonant; spread spectrum; frequency modulation; radiated emissions



Citation: Stepins, D.; Zakis, J.; Padmanaban, P.; Deveshkumar Shah, D. Suppression of Radiated Emissions from Inductive-Resonant Wireless Power Transfer Systems by Using Spread-Spectrum Technique. *Electronics* **2022**, *11*, 730. <https://doi.org/10.3390/electronics11050730>

Academic Editor:
Dominique Schreurs

Received: 30 December 2021

Accepted: 24 February 2022

Published: 26 February 2022

Publisher's Note: MDPI stays neutral with regard to jurisdictional claims in published maps and institutional affiliations.



Copyright: © 2022 by the authors. Licensee MDPI, Basel, Switzerland. This article is an open access article distributed under the terms and conditions of the Creative Commons Attribution (CC BY) license (<https://creativecommons.org/licenses/by/4.0/>).

1. Introduction

Nowadays, one of the popular subfields of electronics and electrical engineering is transferring electric power without wires—wireless power transfer (WPT). It is more reliable and convenient than traditional power transmission with wires.

While a wireless battery charging of mobile electronic devices is often considered as an unnecessary extra, some applications of wireless power transfer should receive attention. They include: wireless charging of the batteries for electrical vehicles [1–3]; wireless charging of mobile robots; wireless charging of the batteries for biomedical implanted devices [4]; dynamic electrical vehicle charging [5]; WPT to moving sensors [6]; WPT to wireless sensor networks nodes [7,8]. WPT also may have some more useful but unusual applications: WPT of solar energy from space to the Earth [9]; wireless charging of the batteries for drones while hovering [10]; wireless charging of the batteries for unmanned autonomous submarines [11,12]; wireless powering of unmanned autonomous aircrafts [13,14].

Currently, the most popular WPT technique is definitely an inductive-resonant WPT technique. It is suitable for small-gap applications [15] when electric power should be transferred wirelessly over a distance up to some 10 s of cm. The inductive-resonant WPT method may be used at low power levels for battery charging of mobile electronic devices or implanted pacemakers as well as at mid and high power levels for the charging of batteries for light-duty electrical vehicles (e.g., passenger cars, etc.) and heavy-duty electrical vehicles (e.g., electrical tractors or buses) as well as mobile robots. Usually, inductive-resonant

WPT systems are designed to operate in kHz range, however sometimes they can also be designed to operate in MHz range (e.g., at 6.78 MHz) to achieve higher transmission distance, better special freedom and lower size. Having switch mode power converters inside, the inductive-resonant WPT systems are potential sources of electromagnetic interference (EMI) to sensitive electronic equipment as shown in Figure 1. EMI can take the form of conducted emissions propagating through input wires to the electric grid and radiated emissions (time-varying magnetic fields or even radio waves) which can even destabilize the normal operation of sensitive electronic devices. Therefore, the emissions must be reduced. This paper is devoted to the reduction of radiated EMI.

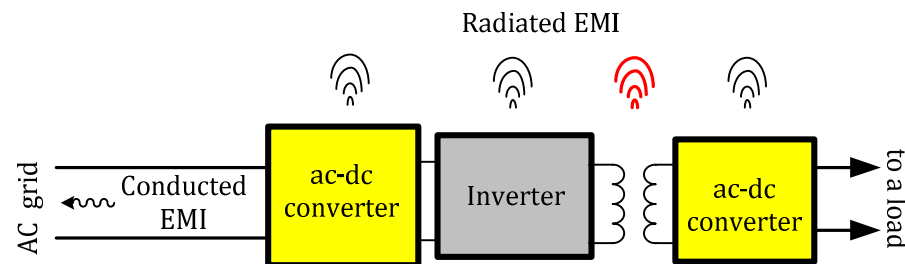


Figure 1. Simplified block diagram of the inductive-resonant WPT system—irradiating electromagnetic emissions.

WPT systems are often considered ISM (industrial, scientific and medicine) devices. Therefore, they should comply with CISPR 11 electromagnetic compatibility (EMC) standard requirements. Since for kHz WPT systems the main emission energy is concentrated within frequency range below 30 MHz, a new CISPR 11 standard edition including guidelines on measurement methods and limits of near-field WPT systems radiated emissions below 30 MHz is due to appear, at the time of writing. Moreover, there is also the International Commission on Non-Ionizing Radiation Protection (ICNIRP) which published guidelines on limiting electromagnetic field exposure.

As a traditional way for conducted EMI reduction—input EMI filtering—adds noticeable cost, size and weight to the inductive-resonant WPT system, a spread-spectrum technique based on modulation of WPT system inverter switching frequency has been applied to inductive-resonant WPT systems [16–22]. A typical approach for the reduction of radiated emissions is shielding, but shields are expensive and they increase the size and cost of the WPT systems. This is the reason why the spread-spectrum approach has been proposed by some researchers.

There are many papers related to the reduction of conducted emissions using a spread-spectrum approach in WPT systems [16–19,21,22], but there is only one paper [20] about the suppression of radiated emissions using the approach in WPT systems. As shown in [20], fundamental components of the radiated emissions of the inductive-resonant WPT system can be reduced by up to 8.3 dB when the spread-spectrum technique based on the random modulation of inverter-switching frequency is used. Despite the fact that the effect of the spread-spectrum technique on the radiated emissions of an inductive-resonant WPT system was analyzed in [20], the research presented in [20] has some drawbacks: (1) only the effect of random frequency modulation on radiated emissions was considered, but the application of classical (periodic) switching frequency modulation (SFM) was not analyzed; (2) the effect of resolution bandwidth (RBW) on the emission measurement results was not taken into account; (3) to implement the modulation, a quite expensive control block based on digital signal processor (DSP) and a field-programmable gate array (FPGA) were used. In contrary to other research [20], the novelty of this paper is an experimentally based analysis of the effect of periodic SFM as well as the multi-frequency technique on radiated emissions of an inductive-resonant WPT system also considering the effects of the RBW of a spectrum analyzer and the efficiency. For the first time it will be shown also that for a similar decrease in the efficiency of the inductive-resonant WPT system, the implementation of the spread-spectrum technique based on the multi-frequency scheme

can lead to a radiated emission reduction equal to or better than that obtained in [20] with random frequency modulation, but using a much cheaper approach—a cheap 8-MHz microcontroller, such as Atmega AVR 328p.

This paper is partly based on the results of a master’s thesis, “Effect of Spread Spectrum Technique on Radiated Emissions Generated by Wireless Power Transfer Systems”, defended by Padmapriya Padmanaban in June 2021 at Riga Technical University under the supervision of D. Stepins.

2. Some Aspects of Periodic SFM and Multi-Frequency Technique

Spread-spectrum techniques based on periodic (classical SFM), random or chaotic SFM applied to conventional switching power converters for conducted emission reduction have been studied quite well during the past 2 decades. Up to the present time, periodic SFM or random SFM have been used also in inductive-resonant wireless power transfer systems, mainly to reduce conducted emissions (however, there is at least one paper [20] considering random SFM for radiated emission reduction).

2.1. Periodic Switching Frequency Modulation

Modulation of the switching frequency of a WPT system high-frequency inverter is usually obtained by the modulating of the inverter control signal frequency. The control signals of the inverters’ switches are usually of square waveform. Basically, a square signal with periodically modulated frequency can be represented by the following formula:

$$s(t) = \text{sign}[\sin(\omega_0 t + 2\pi\Delta f_{\text{peak}} \int_0^t s_{\text{mod}}(\tau) d\tau)], \quad (1)$$

where ω_0 is the central angular frequency ($\omega_0 = 2\pi f_0 t$);

Δf_{peak} is the peak switching frequency deviation;

$s_{\text{mod}}(t)$ is modulation waveform, such as sine, triangle or ramp with unitary amplitude.

Particularly, if $s_{\text{mod}}(t)$ is sine, then Equation (1) can be transformed into a simpler expression:

$$s(t) = \text{sign}[\sin(\omega_0 t + \beta \sin(2\pi f_m t))], \quad (2)$$

where β is frequency modulation index which is the peak frequency deviation ratio to modulation frequency (f_m).

From Equation (1) it follows that a frequency modulated square signal in time domain can be represented also by time instants t_k at which the transitions between low and high levels (and vice versa) occur. The time instants can be calculated by finding the roots of equation $s(t) = 0$ or by simulating the frequency modulator with a square signal as an output. As an example, simulated switching frequency modulated square signal waveform is shown in Figure 2. As is obvious from the figure, the k -th switching periods (T_1, T_2, \dots, T_k) are not equal and the k -th time intervals corresponding to a high-level or low-level voltage, $t_{\text{on},k}$ and $t_{\text{off},k}$, respectively, are not equal within a single modulation period T_m . So, it can be written that within a T_m , $T_1 \neq T_2 \neq T_k$, $t_{\text{on}1} \neq t_{\text{on}2} \neq t_{\text{on},k}$, $t_{\text{off}1} \neq t_{\text{off}2} \neq t_{\text{off},k}$. The time instant values calculated from the simulated waveform (Figure 2) at which the transitions occur are: $t_1 = 0 \mu\text{s}$; $t_2 = 6.541 \mu\text{s}$; $t_3 = 12.908 \mu\text{s}$; $t_4 = 19.115 \mu\text{s}$; $t_5 = 25.217 \mu\text{s}$; $t_6 = 31.106 \mu\text{s}$; $t_7 = 36.889 \mu\text{s}$; $t_8 = 42.513 \mu\text{s}$; $t_9 = 48.083 \mu\text{s}$; $t_{10} = 53.495 \mu\text{s}$; $t_{11} = 58.82 \mu\text{s}$.

It is rather well known that SFM leads to a spectrum-spreading effect, resulting in peak emission level reduction in frequency domain, as may be seen in Figure 3. In order to estimate the phenomenon of the emissions reduction, the radiated EMI reduction coefficient K_{red} (expressed in dB) is used. The coefficient can be defined as a difference between the maximum emission levels (in frequency domain, expressed, e.g., in dB μV or dB $\mu\text{A}/\text{m}$) of a WPT system with and without spread spectrum. As it is shown in [16] or [22] for conducted emissions, the spectrum spreading effect and the peak emissions level reduction associated with it depend on periodic SFM parameters, such as Δf_{peak} , f_m and modulation waveform.

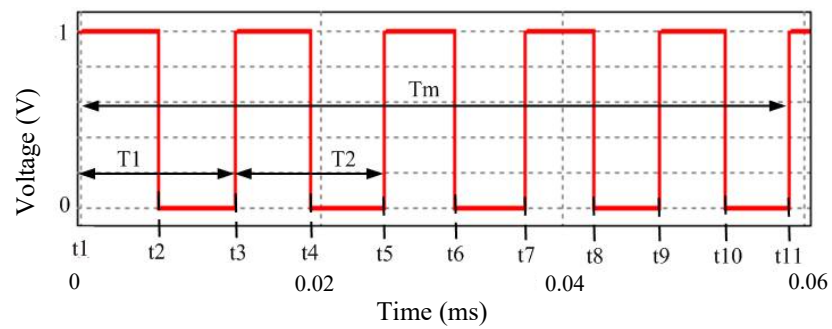


Figure 2. Simulated square control signal waveform with periodic SFM. Parameters: central switching frequency $f_0 = 85$ kHz; $\Delta f_{\text{peak}} = 10$ kHz; $f_m = 17$ kHz. Modulation waveform is ramp.

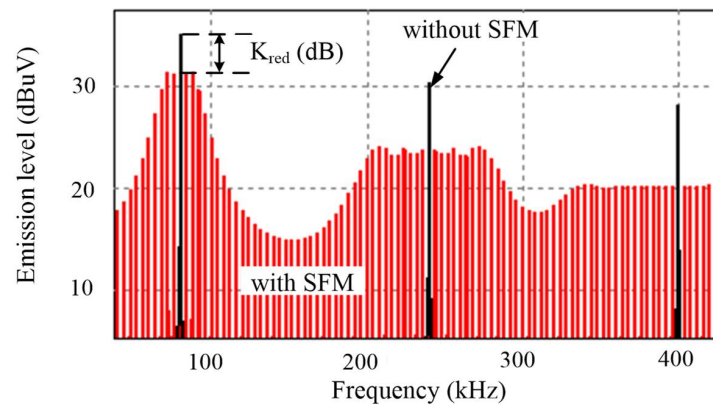


Figure 3. Simulated square signal spectra for two cases: when SFM is not used and when it is used.

2.2. Multi-Frequency Technique

One more spread-spectrum technique related to the periodic SFM is so-called multi-frequency technique. This technique was applied for the first time for the reduction of conducted emissions generated by WPT systems and it is well described in [21]. The spectrum-spreading technique can be considered as a periodic SFM with staircase modulation waveform. In this technique, a WPT system operates at two or more different switching frequencies (f_1, f_2, \dots, f_k). The modulation period T_m comprises k time intervals (τ_k) in which the WPT system operates at different frequencies f_k . One or more switching periods with constant frequency f_k and constant duty cycle could take place at one τ_k , that is depicted in Figure 4. Due to the fact that the WPT system operates at several frequencies, the most significant emission levels are concentrated at f_k and $f_k \pm f_m$ (where $f_m = 1/T_m$). The main parameters characterizing the multi-frequency techniques are: modulation frequency (f_m), the k -th switching frequency f_k , difference between maximum and minimum switching frequency Δf , modulation period T_m .

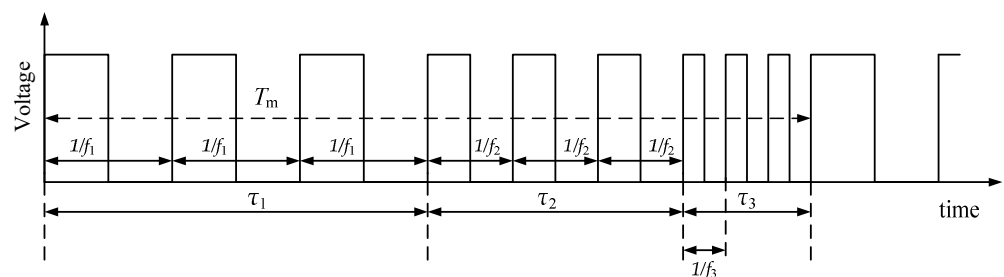


Figure 4. Waveform of square signal with three-switching-frequency technique. During τ_1 the system operates at frequency f_1 , during τ_2 the system operates at frequency f_2 , but during τ_3 the system operates at frequency f_3 .

3. Experimental Setup

In order to study the effect of periodic SFM and multi-frequency technique on the radiated emissions and the efficiency of the inductive-resonant WPT system, an experimental prototype of the system has been designed and practically built. A block diagram of the prototype is depicted in Figure 5. It consists of half bridge inverter (EVB GSWP050W from GaN systems), the half-bridge inverter dead-time control circuit, a microcontroller (ATmega328PB Xplained Mini evaluation board), the primary-side and the secondary-side series compensation circuit (based on parallel connected capacitors to increase overall current rating), inductively coupled coils, secondary-side high-frequency full-wave rectifier with high-frequency ripple filter and step-down regulator at the primary side to feed the microcontroller (MCU), the dead-time control circuit and the inverter GaN transistors drivers. The dead-time control circuit generates two square signals to control the half-bridge stage transistors introducing some delay to prevent the stage from the shoot-through phenomenon. The half-bridge inverter input is connected to the output of the DC power supply whose output voltage can be adjusted. Two parallel connected resistors with suitable heatsink and a cooling fan are used as a load. Transmitting and receiving coils are factory-made ones from Würth Elektronik. The primary and the secondary compensation capacitances were calculated so that the primary and secondary-side resonant tanks are tuned to the resonance (at f_0). The WPT system was designed for the operation within the Qi standard allowed range of frequencies (this is why the central switching frequency f_0 is 150 kHz).

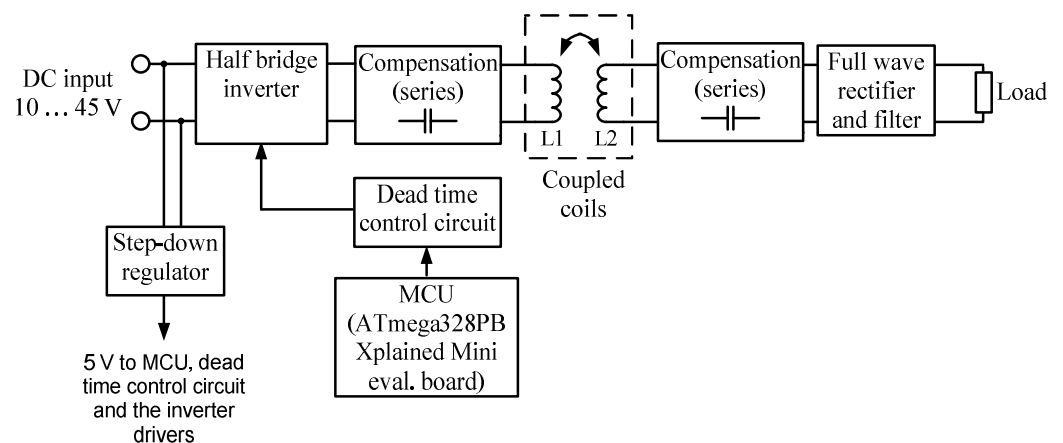


Figure 5. A block diagram of the experimental prototype.

The values of the main parameters of the designed WPT system are shown in Table 1.

Table 1. The designed WPT system parameters values.

Parameter	Numerical Value	Unit of Measurement
Rated output power	31	W
Rated output voltage	10	V
Central switching frequency f_0	150	kHz
Range of allowed input voltages	10 ... 45	V
Range of allowed switching frequencies	120 ... 180	kHz
Transmitting coil inductance	25.07	μH
Receiving coil inductance	25.25	μH
Primary compensation capacitance	44.95	nF
Secondary compensation capacitance	44.63	nF
Range of coupling coefficients	0.21 ... 0.3	-

Since at the time of writing the paper we had only a cheap 8 MHz 8-bit MCU evaluation board, accurate implementation of periodic SFM was impossible, because the MCU time resolution ($1/8 \times 10^6 = 125$ ns) was insufficient to generate frequency-modulated

square signal (e.g., shown in Figure 2) accurately with timings, presented, for example, in Section 2. Therefore, instead of an MCU, a signal generator Tektronix AFG3022C was used to generate square signal with periodic SFM. The signal generator has a built-in frequency modulator mode and all modulation parameters can be set by it. However, multi-frequency technique (with 2–4 switching frequencies) does not require accurate timings and therefore, a cheap low-resolution microcontroller can be used. So, for obtaining a square signal with multiple frequencies as shown in Figure 4, we used the MCU ATmega328PB Xplained Mini evaluation board. For generation of the pulse sequence, a direct MCU port manipulation (using *delay_us*) was used. By composing the MCU program code, modulation (repetition) frequency f_m and maximum difference between switching frequencies $\Delta f = f_{\max} - f_{\min}$ can be simply achieved. Note that when the signal generator was connected to the input of the dead-time circuit, the microcontroller evaluation board was switched off and disconnected from the dead-time control circuit and vice versa.

A photo of the experimental setup is shown in Figure 6. Since at the time of submission of the manuscript the CISPR11 guidelines on limits and measurement methods of the radiated emissions from the inductive-resonant WPT systems were not available, to measure the radiated emissions we used the approach similar to that in [20]: a near-field H probe (Rohde&Schwarz, HZ-14, 9 kHz–30 MHz) connected to a mixed-domain digital oscilloscope Tektronix MDO4034B with separate spectrum analyzer input to analyze radiated magnetic field in the near-field region. Since output quantity of the near field probe is a voltage level V_{probe} (expressed in dB μ V), but we should know the magnetic field strength level H (expressed in dB μ A/m), the near field probe HZ-14 antenna factor AF (taken from the manufacturer datasheet) was added to the output voltage measurement results in dB μ V as follows:

$$H = V_{\text{probe}} + \text{AF}. \quad (3)$$

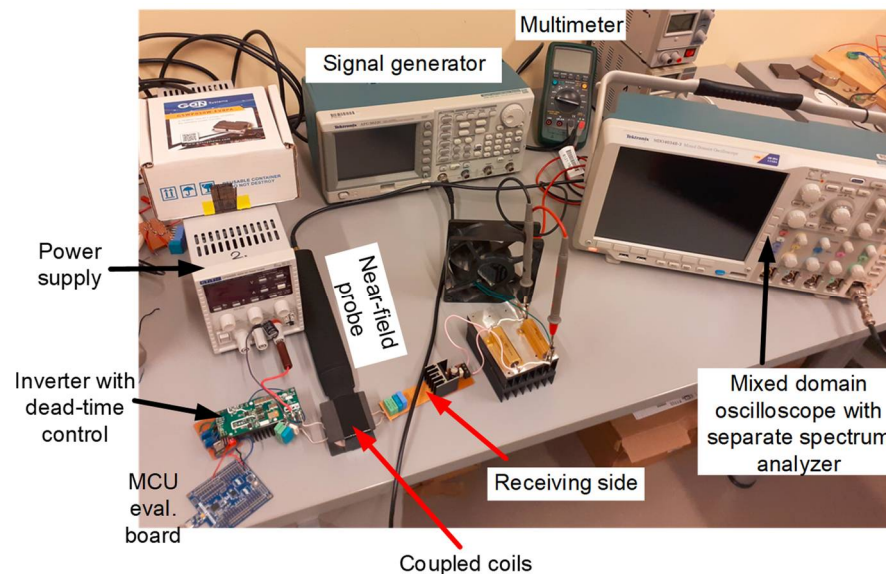


Figure 6. Image of the experimental setup.

The efficiency was calculated as the ratio of measured output real power to measured input real power of the inductive-resonant WPT system.

4. Results and Discussion

The measurements were made within the range 100 kHz . . . 1 MHz, because in this range the most significant emission levels were measured. The measurements were made for a maximum distance between the coils (1.8 cm) that corresponds to the minimum coupling coefficient of 0.21 (because it was experimentally found out that at the maximum

distance between the coils, the radiated emissions levels are the highest). A peak detector was used during the measurements. The obtained results were saved in CSV format files and then postprocessed by using Matlab to take into account the antenna factor of the probe. Since the emission measurement results for $f_m < \text{RBW}$ were very unstable, we did not calculate the radiated emission reduction coefficients in this case. Moreover, when RBW was chosen to be 10 kHz, the results obtained for modulation frequencies below 8 kHz with peak detector and maxHold function were even worse than those without SFM. For $f_m \geq \text{RBW}$, the measurement results were quite stable and peak detector with averaging of 16 consecutive sweeps was used to achieve better accuracy. The measurements were made with three different RBWs, namely, 100 Hz, 1 kHz and 10 kHz.

During the emissions measurements, it was concluded that the main sources of the radiated magnetic fields are the transmitting and the receiving coils. Since we were interested only in relative measurements, a distance (5 mm) between the probe and the coils was chosen so that quite high levels of the magnetic field emissions could be measured.

Despite the fact that the WPT system was examined in an open-loop mode, the output voltage was measured and adjusted to be 10 V (by adjusting the input power supply output voltage) in order to imitate the closed-loop mode with constant output voltage. This action made the comparable measurements under different control schemes possible, because when different spread-spectrum techniques are applied, the output voltage can be changed.

The operation of the signal generator and the power supply does not have any influence on the measured radiated magnetic fields coming from the WPT system under the test. When the WPT system was switched off, the measured emission levels were similar to the noise floor of the spectrum analyzer itself, as may be seen in Figure 7.

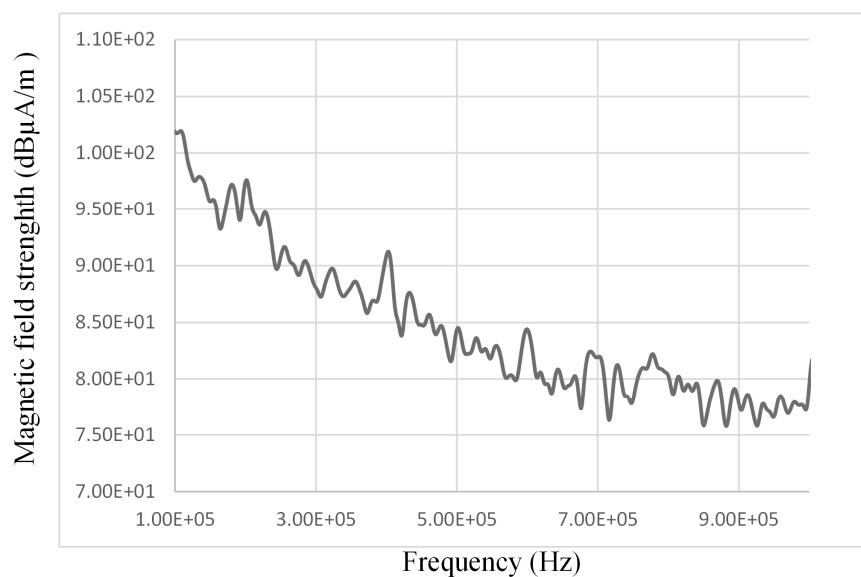
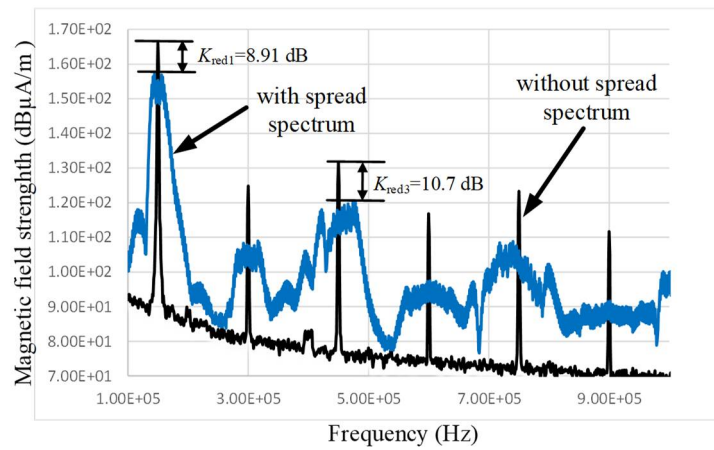
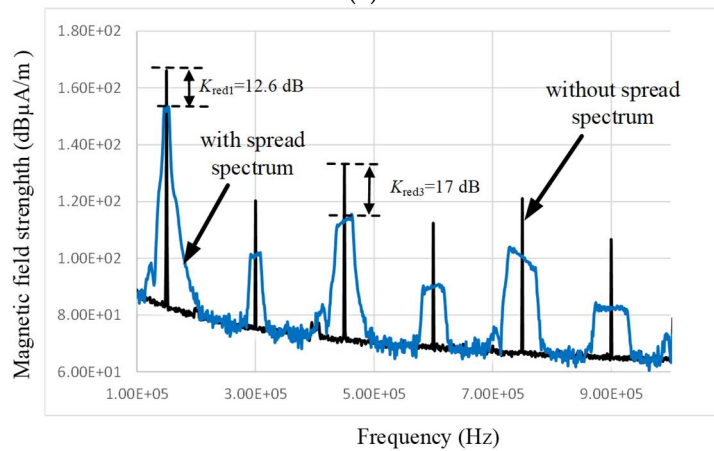


Figure 7. Radiated emission spectrum when the signal generator and the power supply were switched on but the WPT system was switched off.

The radiated emissions measurement results when a periodic SFM (with different f_m , Δf_{peak} and modulation waveforms) and multi-frequency technique (with different f_m and Δf) were used are presented in Figures 8–12, Tables 2 and 3. In addition, the efficiency measurement results are shown in Figures 13–15 and Table 3.

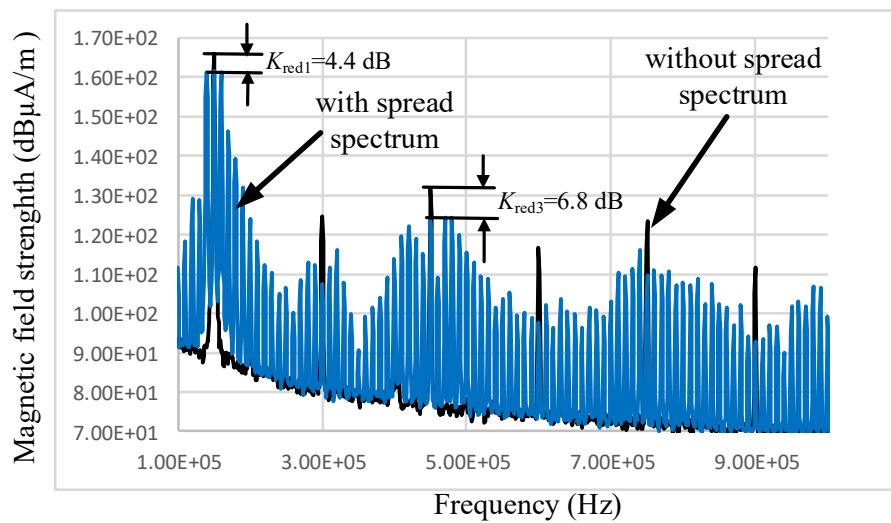


(a)



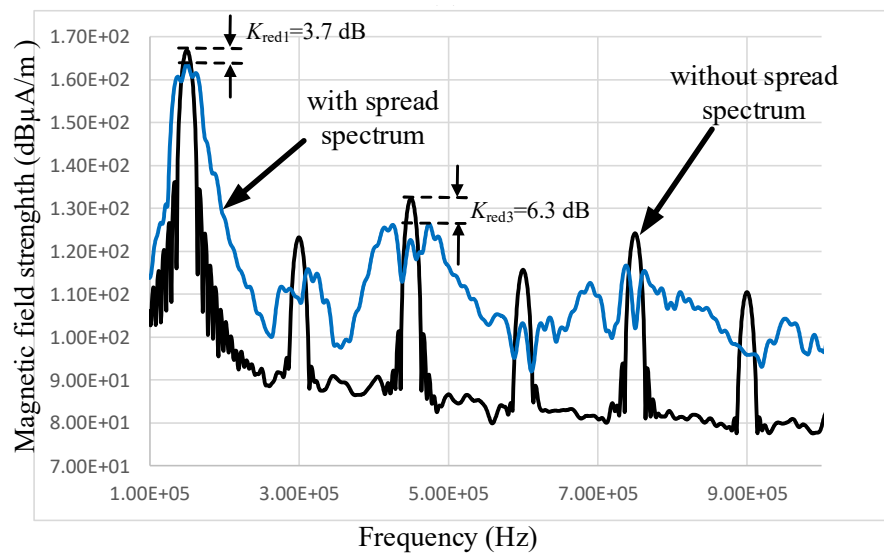
(b)

Figure 8. Comparison of spectra of radiated emissions from the WPT system without spread spectrum and with spread spectrum based on ramp SFM: (a) $f_m = 2$ kHz, $\Delta f_{\text{peak}} = 12$ kHz, RBW = 1 kHz; (b) $f_m = 0.35$ kHz, $\Delta f_{\text{peak}} = 5$ kHz; RBW = 0.1 kHz).



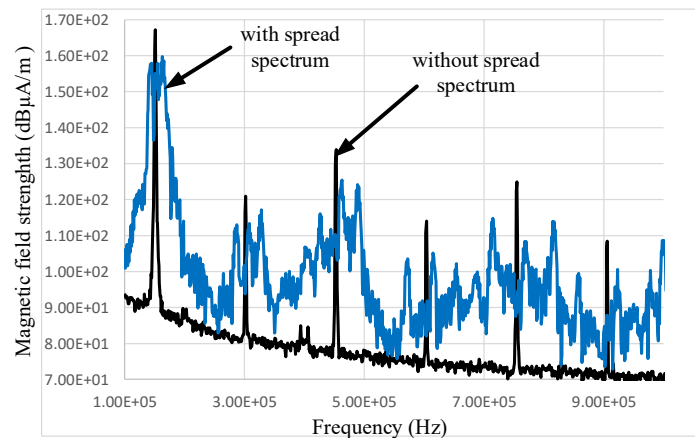
(a)

Figure 9. Cont.

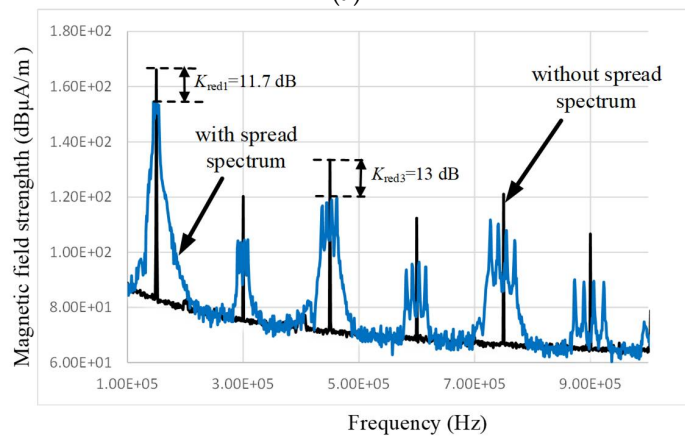


(b)

Figure 9. Comparison of spectra of radiated emissions from the WPT system without spread spectrum and with spread spectrum based on periodic SFM: (a) without SFM and with periodic SFM (sine modulation, $f_m = 10$ kHz, $\Delta f_{\text{peak}} = 12$ kHz; RBW = 1 kHz); (b) without SFM and with periodic SFM (sine modulation, $f_m = 10$ kHz, $\Delta f_{\text{peak}} = 12$ kHz; RBW = 10 kHz).



(a)



(b)

Figure 10. Comparison of spectra of radiated emissions from the WPT system without spread spectrum and with spread spectrum based on multi-frequency technique: (a) 3-frequency technique,

$f_m = 2$ kHz, $f_1 = 140.4$ kHz, $f_2 = 151.1$ kHz, $f_3 = 160.3$ kHz, $\Delta f = 20$ kHz; RBW = 1 kHz; (b) 4-frequency technique, $f_m = 0.35$ kHz, $f_1 = 145.3$ kHz, $f_2 = 148.8$ kHz, $f_3 = 151.1$ kHz, $f_4 = 154.3$ kHz $\Delta f = 9$ kHz; RBW = 0.1 kHz.

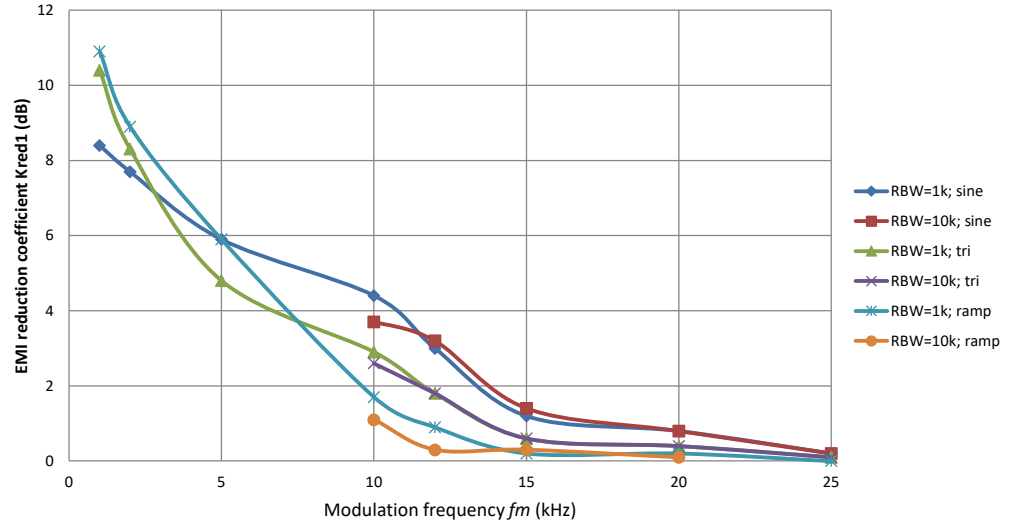


Figure 11. K_{red} versus f_m when periodic SFM (with different modulation waveforms and $\Delta f_{peak} = 12$ kHz) is used.

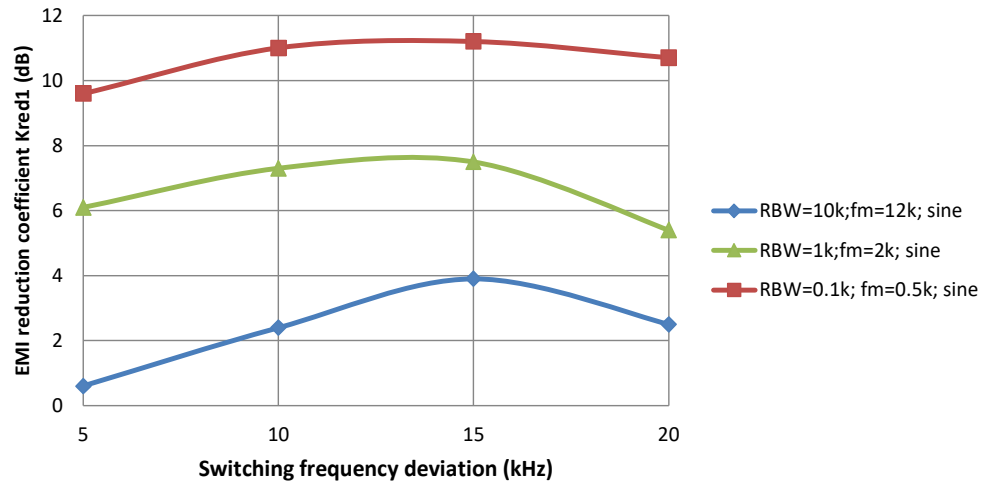


Figure 12. K_{red1} versus Δf_{peak} when periodic SFM (with sine modulation waveform and different f_m) is used.

Table 2. The third harmonic amplitude reduction coefficient (K_{red3}) as a function of f_m (RBW = 1 kHz; $\Delta f_{peak} = 12$ kHz).

Modulation Frequency (kHz)	K_{red3} [dB] for Sine SFM	K_{red3} [dB] for Triangular SFM	K_{red3} [dB] for Ramp SFM
1	10.5	12	12.9
2	9	10.5	10.7
5	6.2	6.1	6.3
12	5.1	5.3	3.4
15	3.1	2.1	3
25	2.4	1.6	1.3

Table 3. Radiated emission reduction coefficients and the efficiency of the WPT system under the measurements with three-switching-frequency technique used. Note: when $f_m = 2$ or 5 kHz, then RBW was chosen to be 1 kHz; when $f_m = 0.5$ or 0.35 kHz, then RBW = 0.1 kHz.

Scheme Type	K_{red1} (dB)	K_{red3} (dB)	Efficiency (%)
3-switching frequency ($f_1 = 130.9$ kHz, $f_2 = 151.5$ kHz, $f_3 = 170.1$ kHz, $f_m = 2$ kHz)	6.5	9.6	67.2
3-switching frequency ($f_1 = 130.9$ kHz, $f_2 = 151.5$ kHz, $f_3 = 170.1$ kHz, $f_m = 5$ kHz)	5.4	9.4	67.6
3-switching frequency ($f_1 = 140.4$ kHz, $f_2 = 151.5$ kHz, $f_3 = 160.3$ kHz, $f_m = 2$ kHz)	7.9	9.3	72.1
3-switching frequency ($f_1 = 145.3$ kHz, $f_2 = 151.5$ kHz, $f_3 = 156.3$ kHz, $f_m = 0.5$ kHz)	9.1	9.5	75.97
4-switching frequency ($f_1 = 145.3$ kHz; $f_2 = 148.8$ kHz; $f_3 = 151.5$ kHz; $f_4 = 154.3$ kHz; $f_m = 350$ Hz)	11.7	13	76.48

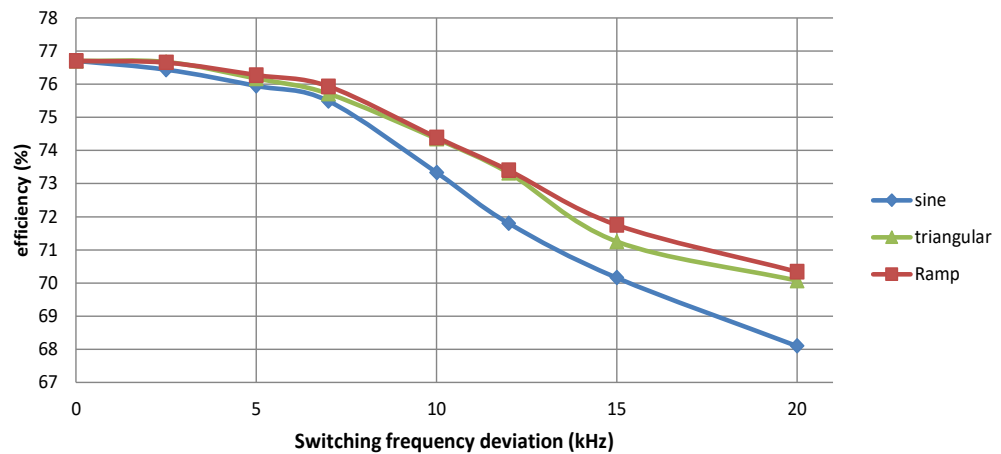


Figure 13. Measured efficiency versus Δf_{peak} when periodic SFM (with different modulation waveforms and $f_m = 1$ kHz) is used. Note: the efficiency of the WPT system without the spread spectrum is 76.7%.

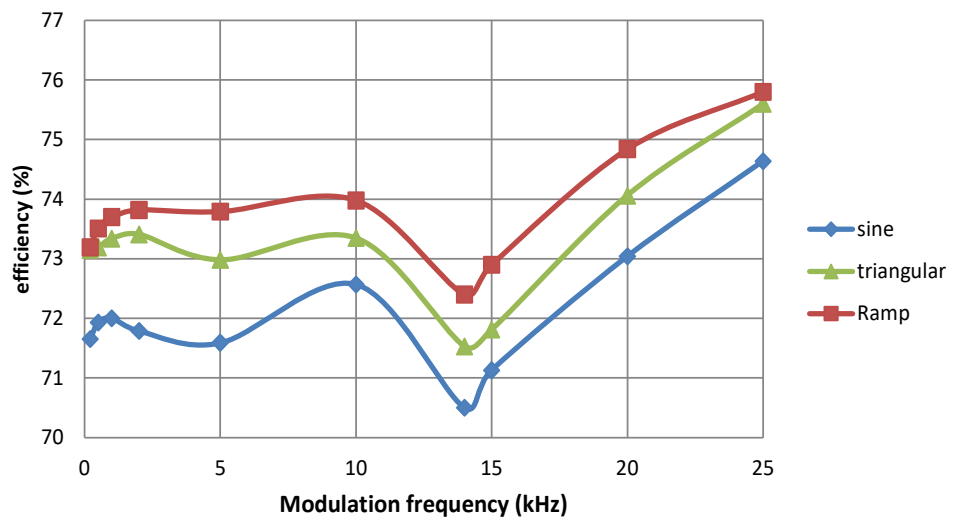


Figure 14. Measured efficiency versus f_m when periodic SFM (with different modulation waveforms and $\Delta f_{peak} = 12$ kHz) is used. Note: the efficiency of the WPT system without the spread spectrum is 76.7%.

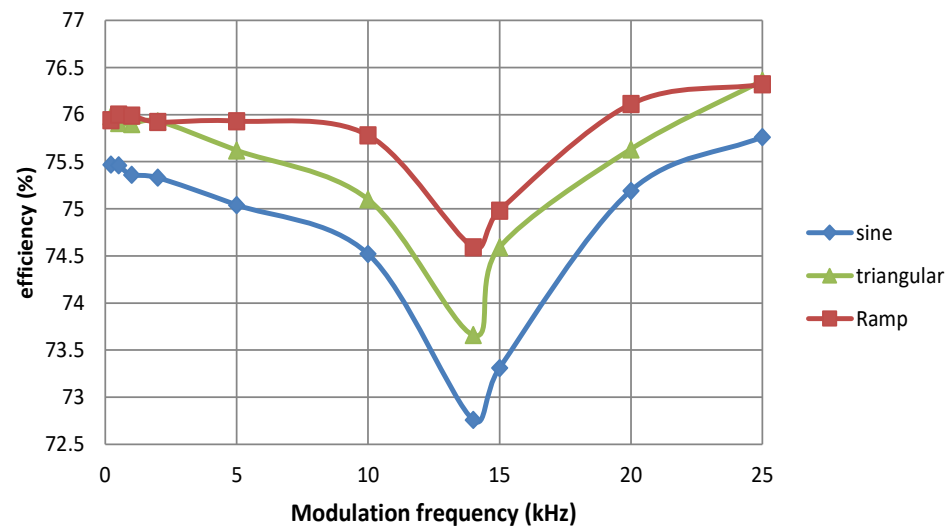


Figure 15. Measured efficiency versus f_m when periodic SFM (with different modulation waveforms and $\Delta f_{\text{peak}} = 5$ kHz) is used.

4.1. Analysis of the Radiated Emissions Measurement Results

As may be seen from these results, both periodic SFM and multi-frequency techniques lead to a noticeable radiated magnetic fields reduction (when $f_m > \text{RBW}$) as shown in Figures 8–12. However, when f_m is lower than RBW, then no reduction can be observed. Sometimes, the peak radiated emissions levels may be even higher than those measured without the spread spectrum, because many spectrum components appear within the bandwidth of an intermediate filter of the spectrum analyzer in this case and, therefore, it is not able to distinguish the adjacent spectrum components which are f_m apart. Moreover, as can be seen in Figure 9, when $\text{RBW} = 10$ kHz, then spectrum components of the radiated emissions of the WPT system without the spread spectrum were visually wider when compared to that if $\text{RBW} = 1$ kHz. In an ideal case, a spectrum component should be a vertical line. As RBW of an intermediate filter of the spectrum analyzer increases, “width” of the spectrum components on the analyzer screen also increases. In Figure 9b, we can see also that when spread spectrum is used and if f_m is not much higher than RBW, then we cannot see vertical spectrum lines, but we see an envelope (blue line in Figure 9b).

In order to quantitatively assess the radiated emission reduction, fundamental emission harmonic and the third emission harmonic amplitudes reduction coefficients, K_{red1} and K_{red3} , respectively, were calculated from the measurements, because these harmonics are the most dominant ones (especially the first harmonic).

For periodic SFM, the coefficients of the radiated emission reduction are the functions of SFM parameters: f_m , Δf_{peak} and modulation waveforms. The reduction of the amplitudes of the radiated emission higher-order harmonics is better than the reduction of the fundamental harmonic amplitude (see e.g., Figure 8) in the frequency range of interest for all modulation waveforms. The multi-frequency technique also gives better reduction of the amplitudes of higher-order harmonics than the reduction of the fundamental one (Figure 10). At high modulation indexes ($\beta = \Delta f_{\text{peak}}/f_m > 2.5$), the ramp SFM is the best choice, but at lower β sine SFM is the best choice (see Figure 11). As the modulation frequency increases, the radiated emissions reduction becomes worse. This, actually, coincides with the Bessel functions theory: higher arguments (β) of the Bessel functions give lower values of the functions.

However, the dependence of the fundamental harmonic reduction coefficient K_{red1} on Δf_{peak} is more interesting: K_{red1} improves as Δf_{peak} increases, but when Δf_{peak} exceeds 13–16 kHz, the emissions reduction worsens (Figure 12). Increasing of K_{red1} with Δf_{peak} increasing is logical and can be easily described by the Bessel functions theory. However, why does the emission reduction become smaller at high Δf_{peak} ? This can be described

by the interaction between the SFM and the WPT system operating with the coupling coefficient larger than its critical value. When coupling coefficient between the receiving and transmitting coils is above its critical value, then well-known “frequency splitting phenomena” takes place, due to which there are two output power (and the coils’ currents) peaks. For the WPT system under the study, there are two output power maxima at frequencies 149 ± 13 kHz (at 149 kHz there was power minimum) when $k = 0.21$. Since the main power of modulated emissions lies within the bandwidth of $2\Delta f_{\text{peak}}$ (for fundamental frequency component), for Δf_{peak} exceeding 13 kHz, the frequency components of the emissions due to the modulations appearing in the vicinity of the output power maxima can be significantly amplified owing to the frequency splitting phenomenon. As a result, there is worsening of the radiated emissions reduction coefficient K_{red1} observed for $\Delta f_{\text{peak}} > 12$ kHz. However, it is very important to note that the higher-order harmonics reduction coefficients improve, as Δf_{peak} increase even up to $\Delta f_{\text{peak}} = 30$ kHz. The reason for this is that the frequency splitting phenomenon does not occur at these frequencies.

For $f_m > \text{RBW}$, the emissions reduction coefficients have almost the same values regardless of RBW value for a given value of f_m and Δf_{peak} (Figure 11).

For the multi-frequency scheme, lower value of f_m gives better K_{red1} (correct only if $f_m \geq \text{RBW}$) as may be seen in Table 3. Reduction of the higher-order harmonics is better than that of the fundamental harmonic within frequency range of interest (see Table 3). The 4-frequency technique provides better K_{red1} and K_{red3} than 3-frequency technique for the same Δf .

4.2. Analysis of the Efficiency Measurement Results

Along with the positive effect in terms of the radiated emissions reduction, the periodic SFM and the multi-frequency technique, unfortunately, can lead to a noticeable reduction of the WPT system efficiency (Figures 13–15 and Table 3).

Similar to the radiated emissions reduction coefficients, the efficiency also is the function of modulation parameters: modulation waveform, f_m , Δf_{peak} and Δf .

As Δf_{peak} (for SFM) or Δf (for the multi-frequency scheme) increase, the efficiency decreases (Figure 13 and Table 3). The decrease in the efficiency can be quite significant (it can even exceed 6% for sine modulation and the multi-frequency technique) at higher Δf_{peak} or Δf . If Δf_{peak} is quite low (<6 kHz), then there is insignificant decrease in the efficiency (below 1%) for all modulation waveforms as it may be seen in Figure 13. Note that the efficiency of the WPT system without the spread spectrum is 76.7% for both the periodic SFM and the multi-frequency technique.

The efficiency is in quite complex relationship with f_m as it may be seen in Figures 14 and 15. A huge drop in the efficiency can be observed if f_m is equal to frequencies (or in the vicinity of them) at which the output power is maximum. This “side effect” can be explained by the fact that the RMS values of the power components’ currents increase significantly (and as the result the power components’ losses also increase) at those frequencies. The efficiency worsens insignificantly, if quite high modulation frequencies (>22 kHz) are used, but, unfortunately, the radiated emissions reduction may be poor, if quite large f_m is used (see Figure 11).

Ramp modulation waveform is not only the best choice in terms of the radiated emission reduction when $\beta > 2.5$, but also it is the best choice in terms of the efficiency, because it gives the lowest drop in the efficiency for different f_m and Δf_{peak} (Figures 13–15). Sine modulation gives the worst results in terms of the efficiency. However, sine modulation gives better reduction of the radiated emissions when $\beta < 2.5$.

The multi-frequency scheme also results in a noticeable decrease in the efficiency (Table 3) especially for higher Δf values. For a given value of the efficiency, the multifrequency scheme (based either on 3 or 4 frequencies) gives equal or slightly higher coefficients of the radiated emission reduction than SFM with sine modulation waveform, but it gives, by 1–3 dB, lower radiated emission reduction than in the case of SFM with ramp waveform.

The presented results allow us to conclude that there is trade-off between the radiated emission reduction and the efficiency, because better reduction of the emissions can be achieved at higher peak switching frequency deviations for a given value of f_m (this conclusion is valid only when Δf_{peak} is below the frequency at which the output power is maximum), but higher Δf_{peak} gives higher drop in the efficiency.

4.3. Choice of the Spread-Spectrum Technique and Its Parameters

At the inductive-resonant WPT system design stage, it is of importance to know what spread-spectrum technique (either periodic SFM, multi-frequency technique or random frequency modulation investigated in [20]) and its parameters should be selected to obtain a quite significant reduction of the radiated emissions with an allowed drop in the efficiency.

As may be deduced from the results obtained in this paper and in [20], the periodic SFM and the multi-frequency techniques may give equal or even better reduction of the radiated emissions when compared to that of the random frequency modulation (presented in [20]) for a given value of RBW (according to the authors [20] information, the RBW during their experiments was 100 Hz) and decrease in the efficiency, but the implementation of the periodic SFM and the multi-frequency scheme is simpler and cheaper.

Please note that to implement the periodic SFM, a microcontroller with quite good time resolution is necessary (CPU clock frequency should be at least 32 MHz), but to implement the multi-frequency technique a microcontroller with 8 MHz CPU clock frequency is enough. However, according to manufacturers' price lists, the cost of a microcontroller does not depend on CPU frequency significantly. Therefore, even if the periodic SFM requires a microcontroller with higher CPU clock frequency, the implementation cost will be slightly higher than that of the multi-frequency scheme.

4.3.1. Choice of the Spread-Spectrum Technique

Obviously, if the cost of the control stage is very important, then it is better to choose either the periodic SFM or the multi-frequency technique as the spread-spectrum technique to reduce the radiated emissions from the inductive-resonant WPT systems. If microcontrollers with at least 32 MHz CPU clock frequency are available, then it is better to implement periodic SFM with ramp modulation waveform, because the periodic SFM with ramp modulation waveform outperforms the multi-frequency technique moderately.

4.3.2. Choice of the Modulation Frequency for the Periodic SFM

The choice of f_m is limited by RBW which is required by an EMC standard. The modulation frequency should be chosen so that $f_m \geq \text{RBW}$. If the radiated emissions measurements should be made with, for example, $\text{RBW} = 9 \text{ kHz}$, then f_m should be e.g., 10 kHz. The modulation frequency should never be chosen in the vicinity of the frequency at which output power is maximum.

4.3.3. Choice of the Modulation Waveform for the Periodic SFM

If $\Delta f_{\text{peak}}/f_m > 2.5$, then ramp modulation waveform should be chosen. For lower values of the modulation index it is better to use the sine modulation.

4.3.4. Choice of the Switching Frequency Deviation for the Periodic SFM

The switching frequency deviation should be chosen as high as possible to get sufficient radiated emissions reduction, but below its threshold value at which the drop in the efficiency is maximum allowable (at the lowest coupling coefficient).

4.3.5. Choice of Parameters for the Multi-Frequency Technique

It is necessary to choose only two parameters for the multi-frequency scheme: modulation frequency f_m and difference between maximum and minimum switching frequency Δf . The choice of the parameters (f_m and $\Delta f = 2\Delta f_{\text{peak}}$) for the multi-frequency scheme is the same as in the case of the periodic SFM: f_m should be equal or higher than RBW, but

Δf should be as high as possible, but below its threshold value at which the drop in the WPT system efficiency is maximum allowable (at the lowest coupling coefficient). f_m should never be chosen close to the frequency at which output power is maximum. It is better to choose the four-frequency technique than the three-frequency technique.

5. Conclusions

For the first time, a detailed analysis of the influence of periodic SFM and multi-frequency technique parameters on inductive-resonant WPT systems' radiated emissions and their efficiency has been performed in this paper.

The obtained results show that both the periodic SFM and the multi-frequency technique can be very useful to reduce the radiated emissions from the inductive-resonant WPT systems, but there is trade-off between the inductive-resonant WPT system radiated emission reduction coefficients and the efficiency that are the functions of either the periodic SFM or the multi-frequency techniques parameters. Some useful recommendations on correct selection of the periodic SFM and the multi-frequency technique parameters presented in the paper can help an engineer to get better inductive-resonant WPT system performance.

Both the periodic switching frequency modulation and the multi-frequency technique are significant competitors of random frequency modulation to reduce radiated emissions of the inductive-resonant WPT systems in the case when their parameters are chosen correctly.

Overall, for a given value of the efficiency, the multi-frequency scheme (based either on 3 or 4 frequencies) gives equal or slightly higher coefficients of the radiated emission reduction than SFM with sine modulation waveform, but it gives, by 1–3 dB, lower radiated emission reduction than in the case of SFM with ramp waveform. As an obvious advantage of the multi-frequency technique is that it can be implemented even using a cheap 8-bit 8-MHz microcontroller.

Author Contributions: Conceptualization, D.S.; methodology, D.S. and P.P.; software and design, D.D.S.; validation, P.P. and D.S.; formal analysis, D.S. and P.P.; data curation, P.P.; writing—original draft preparation, D.S.; writing—review and editing, J.Z.; visualization, J.Z.; supervision, J.Z.; project administration, J.Z. All authors have read and agreed to the published version of the manuscript.

Funding: This work has been supported by the European Regional Development Fund within the Activity 1.1.1.2 “Post-doctoral Research Aid” of the Specific Aid Objective 1.1.1 “To increase the research and innovative capacity of scientific institutions of Latvia and the ability to attract external financing, investing in human resources and infrastructure” of the Operational Programme “Growth and Employment” (No.1.1.1.2/VIAA/3/19/415).

Institutional Review Board Statement: Not applicable.

Informed Consent Statement: Not applicable.

Data Availability Statement: Data of our study are available upon request.

Acknowledgments: We would like to thank Latvian Electronic Equipment Testing Centre (LEETC) technical director G. Asmanis for his help in measuring radiated emissions in LEETC. We would like also to express our gratitude to A. Zhiravecka for her help in improving English grammar.

Conflicts of Interest: The authors declare no conflict of interest.

References

1. Qu, X.; Han, H.; Wong, S.C.; Tse, C.K.; Chen, W. Hybrid IPT Topologies with Constant Current or Constant Voltage Output for Battery Charging Applications. *IEEE Trans. Power Electr.* **2015**, *30*, 6329–6337. [[CrossRef](#)]
2. Bosshard, R.; Kolar, J.W. Inductive power transfer for electric vehicle charging: Technical challenges and tradeoffs. *IEEE Power Electr. Mag.* **2016**, *3*, 22–30. [[CrossRef](#)]
3. Wang, Z.; Wei, X.; Dai, H. Design and Control of a 3 kW Wireless Power Transfer System for Electric Vehicles. *Energies* **2016**, *9*, 10. [[CrossRef](#)]

4. Lenaerts, B.; Puers, R. *Omnidirectional Inductive Powering for Biomedical Implants*; Springer Science: Dordrecht, Germany, 2009; p. 10.
5. Chen, K.; Cheng, K.; Yang, Y.; Pan, J. Stability Improvement of Dynamic EV Wireless Charging System with Receiver-Side Control Considering Coupling Disturbance. *Electronics* **2021**, *10*, 1639. [[CrossRef](#)]
6. Boeij, J.; Lomonova, E.; Duarte, J.L.; Vandenput, A.J. Contactless power supply for moving sensors and actuators in high-precision mechatronic systems with long-stroke power transfer capability in x–y plane. *Sens. Actuators A Phys.* **2008**, *148*, 319–328. [[CrossRef](#)]
7. Xie, L.; Shi, Y.; Hou, Y.T.; Lou, W. Wireless power transfer and applications to sensor networks. *IEEE Trans. Wirel. Commun.* **2013**, *20*, 140–145. [[CrossRef](#)]
8. Lu, X.; Wang, P.; Niyato, D.; Kim, D.I.; Han, Z. Wireless networks with RF energy harvesting: A contemporary survey. *IEEE Commun. Surv. Tutor.* **2015**, *17*, 757–789. [[CrossRef](#)]
9. Satavekar, S.G. Solar Power Satellites and Microwave Wireless Power Transmission Technology. *Adv. Electron. Electr. Eng.* **2014**, *4*, 193–200. [[CrossRef](#)]
10. Coxworth, B. Drone Receives Wireless Power, on the Fly. 2016. Available online: <https://newatlas.com/wireless-power-drones/46030/> (accessed on 23 December 2021).
11. Zhengchao, Y.; Song, B.; Zhang, Y.; Zhang, K.; Mao, Z.; Hu, Y. A Rotation-Free Wireless Power Transfer System with Stable Output Power and Efficiency for Autonomous Underwater Vehicles. *IEEE Trans. Power Electr.* **2019**, *34*, 4005–4008. [[CrossRef](#)]
12. Yoshida, S.; Tanomura, M.; Hama, Y.; Hirose, T.; Suzuki, A.; Matsui, Y.; Sogo, N. Underwater wireless power transfer for non-fixed unmanned underwater vehicle in the ocean. In Proceedings of the International Conference 2016 IEEE/OES Autonomous Underwater Vehicles (AUV), Tokyo, Japan, 6–9 November 2016; pp. 177–180. [[CrossRef](#)]
13. NASA. Nasa Research Team Successfully Flies First Laser-Powered Aircraft. 2003. Available online: http://www.nasa.gov/vision/earth/improvingflight/laser_plane.html (accessed on 28 December 2021).
14. Aldhafer, S. Design and Optimization of Switched-Mode Circuits for Inductive Links. PhD Thesis, Cranfield University, Bedford, UK, 2014.
15. Dai, J.; Ludois, D.C. A Survey of Wireless Power Transfer and a Critical Comparison of Inductive and Capacitive Coupling for Small Gap Applications. *IEEE Trans. Power Electr.* **2015**, *30*, 6017–6029. [[CrossRef](#)]
16. Stepins, D.; Zakis, J.; Audze, J.; Husev, O.; Pakhaliuk, B. Comparative Analysis of Different Spread-Spectrum Techniques for Reduction of Conducted Emissions Generated by Magnetic Resonant Wireless Power Transfer Systems. In Proceedings of the IEEE 2nd Ukraine Conference on Electrical and Computer Engineering (UKRCON), Lviv, Ukraine, 2–6 July 2019; pp. 448–454. [[CrossRef](#)]
17. Suzuki, M. Conducted Emission in an 85 kHz, 50 kW WPT System with Opposite-Phase Transfer and Spread Spectrum. In Proceedings of the 2019 IEEE PELS Workshop on Emerging Technologies: Wireless Power Transfer (WoW), London, UK, 18–21 June 2019; pp. 1–4. [[CrossRef](#)]
18. Nikhil, C.T. EMI Suppression in Inductive Resonant Wireless Power Transfer Systems Using Variable Pulse width Technique. Master Thesis, Riga Technical University, Riga, Latvia, 2019.
19. Kim, M.; Park, H.P.; Jung, J.H. Wireless Power Transfer System with Reduced EMI Emission Employing Spread Spectrum Technique. In Proceedings of the IEEE PELS Workshop on Emerging Technologies: Wireless Power Transfer, Seoul, Korea, 15–19 November 2020; pp. 370–373. [[CrossRef](#)]
20. Inoue, K.; Kusaka, K.; Itoh, J. Reduction in Radiation Noise Level for Inductive Power Transfer Systems using Spread Spectrum Techniques. *IEEE Trans. Power Electr.* **2018**, *33*, 3076–3085. [[CrossRef](#)]
21. Stepins, D.; Akunuri, L.; Subbarao, A.; Zakis, J. Reduction of Electromagnetic Emissions Generated by Inductive Resonant WPT Systems Using Multi-Switching-Frequency-Based Method. In Proceedings of the IEEE 61st International Scientific Conference on Power and Electrical Engineering of Riga Technical University (RTUCON), Riga, Latvia, 5–7 November 2020; pp. 1–8. [[CrossRef](#)]
22. Stepins, D.; Kathari, N.; Zakis, J.; Husev, O.; Pakhaliuk, B.; Shevchenko, V. Effect of Hybrid Modulation on Performance of Wireless Battery Charger Operating in CC/CV Mode. In Proceedings of the 47th Annual Conference of the IEEE Industrial Electronics Society, Toronto, ON, Canada, 13–16 October 2021; pp. 1–6. [[CrossRef](#)]